AUT Journal of Mechanical Engineering

AUT J. Mech. Eng., 7(1) (2023) 3-18
DOI: 10.22060/ajme.2022.21605.6041

An investigation of pool boiling under alternating magnetic field and steady-state conditions

Abutaleb Ramezani[1], Ahmadreza Faghih Khorasani[1]*, Ahmadreza Ayoobi[2]

[1] Department of Mechanical Engineering, Yazd University, Yazd, Iran
[2] Department of Aerospace Engineering, Shahid Sattari Aeronautical University of Science and Technology, Tehran, Iran

ABSTRACT: Applying an alternating magnetic field around the pool boiling region has various effects on the pool boiling's major characteristics. Steady-state pool boiling experiments were performed with deionized water under atmospheric pressure and the application of an alternating magnetic field. A nickel-chrome wire with a diameter of 0.1 mm was used as a heater. Two Helmholtz coils were used to generate the magnetic field. The effects of applying this field with intensities of 5.8, 8.9, and 13.3 mT on pool boiling parameters were investigated in experiments and compared to the state without a magnetic field. The results show that, in general, the application of a magnetic field shortens the pool boiling process and delays the start of the nucleate boiling regime. The critical heat flux did not vary significantly when alternating magnetic fields were used. In comparison to no magnetic field application, this parameter decreased by 1.38%, 2.31%, and 3.33% at magnetic field intensities of 5.8, 8.9, and 13.3 mT. But the boiling heat transfer coefficient has increased to a maximum of 47% at the critical heat flux point. The Lorentz force acting on water molecules reduced the number of bubbles surrounding the wire heater, allowing the heat produced to be transferred to the surrounding liquid more quickly. As a result, the heat transfer coefficient increased with increasing magnetic field strength.

Review History:

Received: Jul. 17, 2022
Revised: Sep. 24, 2022
Accepted: Nov. 16, 2022
Available Online: Nov. 20, 2022

Keywords:

Pool boiling
Alternating magnetic field
Critical heat flux
Heat transfer coefficient
Lorentz force

1- Introduction

Pool boiling is one of the most effective methods of heat transfer, which has been used in various fields such as air conditioning equipment and refrigerators. Therefore, to achieve the highest efficiency, it is necessary to study how to increase the effective parameters in the boiling process. The nucleate boiling regime is significant in the analysis of pool boiling because it is a particularly effective heat transfer mechanism. However, the heat flux must be kept slightly lower than the CHF[1] since, beyond this point, the boiling transitions from the nucleate to a film regime having inadequate heat transfer. Increasing the CHF is a suitable solution to compress and reduce the dimensions of systems using the boiling heat transfer mechanism. This increment also results in higher heat transmission, which improves cooling system efficiency. Recent researches has looked at a variety of methods for enhancing boiling heat transfer in both steady and transient conditions. These methods are split into two categories: active and inactive. Active methods include evaluating the impact of applying a magnetic field on the macroscopic structure of the base fluid [1], applying surface or fluid vibration [2-4], and evaluating the effect of pressure on the boiling parameters [5, 6]. Inactive methods include the morphological effects of the heating surface [7-10] and the effect of employing nanoparticles in the base fluid [11-15]. In this context, the behavior of bubbles [16-18] in various stages of boiling has also been evaluated.

The use of magnetic fields in various forms is one of the ways for improving heat transfer, particularly CHF. Magnetic fields alter the conductivity of electrolyte solutions as well as the amount of evaporated water, according to the previous findings. The effect of these changes are function of the thickness of the hydration shell around the ions and the thermodynamic behavior of the hydration and depend on the nature of the ions present in the solutions [19]. In previous studies, the investigation of the effect of magnetic fields on the pool boiling process has often been done by using permanent magnets on the sides of the heater. For example, Mohammadpourfard *et al.* [14] numerically studied nucleate pool boiling heat transfer of ferrofluids on a horizontal plate under magnetic field gradients. Their results showed that pool boiling heat transfer coefficients of ferrofluids were higher than water, and the presence of magnetic field had a positive effect on nucleate pool boiling heat transfer. Khoshmehr *et al.* [20] experimentally investigated boiling on a Silver cylinder with aspect ratio of 10 and surface roughness of 689 nm. Water and ferrofluid in two different concentrations were used in the presence/absence of a magnetic field in these experiments. They found that CHF was increased by 50% in the presence of the magnetic field. Mahmoudi and Abu-nada [21]

1 Critical Heat flux

*Corresponding author's email: faghih@yazd.ac.ir

numerically studied natural convective heat transfer of CuO/water nanofluids subjected to a magnetic field. They observed that strong magnetic fields would be effective and practical in increasing heat transfer performance of nanofluids. Naphon [15] used a magnetic field with three different strengths of 5,7.5 and 10 mT by a permanent magnet on the surface of the heater. The heater was immersed in pure R141b base fluid and Tio_2 / R141b nanofluid with volumetric concentrations of 0.01%, 0.025%, and 0.05%. According to his findings, in pure refrigerant boiling, magnetic fields have no significant effect on the BHTC[1], but in nanofluids, the boiling heat transfer coefficient increases as the magnetic field intensity increases. Abdollahi *et al.* [22] conducted pool boiling experiments using Fe_3O_4/water nanofluids at various concentrations in a study. To create a uniform magnetic field, two permanent magnets were employed. The overall results showed that the presence of positive and negative magnetic field gradients decrease and increase the boiling heat transfer, respectively. Also, at higher concentrations of nanofluid, the effect of the magnetic field on nanoparticles is boosted. Ayoobi *et al.* [23] investigated the effect of applying a permanent magnetic field on the transient pool boiling process of saturated ionized water under atmospheric conditions with a horizontal wire heater. The results demonstrated that the CHF occurs at a higher wall superheated temperature in the presence of a permanent magnetic field. In the presence of a magnetic field, CHF values in periods of 100 and 1000 seconds were greater than corresponding values in the absence of a magnetic field, which could be because of changes in the chemical-physical properties of magnetized water. The increase in heat flux due to the presence of a magnetic field for a time period of 100s and 1000s was found to be 12.74% and 7.3%, respectively. Lykoudis [24] showed that applying a magnetic field to the boiling of metal elements such as mercury and potassium, reduces bubbles development. As a result, the overall rate of heat transfer is reduced.

A small number of previous studies have looked into the effect of homogeneous and heterogeneous fields caused by the pass of electric current in a conductive wire on the process of pool boiling. Using a copper wire with a diameter of 50μm in a channel-shaped cell with a circular cross-section, Vatani *et al*. [25] established an electric current (1.5-3 A). A magnetic ferrofluid was considered to be the working fluid. It was discovered through several experiments using various electric currents that increasing the current, enhances the capability of heat transfer. When a non-uniform magnetic field is applied to the heater in a pool boiling, the heat transfer changes differ from when a uniform magnetic field is applied. For example, Lee *et al*. [26] used a 0.01 *mm* diameter and 3 *mm* length platinum wire inside a steel tube carrying a magnetic Fe_3O_4 / Water fluid to apply heat to the fluid. A solenoid was used to apply uniform and non-uniform magnetic fields. The results demonstrated that providing a uniform magnetic field reduces heat transfer between the wire heater and the fluid due to increase of magnetic field's viscosity. The heat transfer between the wire heater and the fluid is boosted because of the Kelvin auxiliary force accelerates the flow of the magnetized fluid when a non-uniform magnetic field (gradient) is applied.

In all recent boiling research, magnetic fields are used in the form of permanent magnets, DC solenoids, or heterogeneous fields. But in this research, for the first time, the authors have used a new method of moving and changing the direction of the field using AC, which is in the form of frequency. Also, in this research, the design was based on the production of the magnetic field only around the wire heater and was not extended to the rest of the field. Therefore, the main focus and the most movement and change of field direction was only in a range close to the wire. Although other areas will face a lesser level of these changes. But the goal was only to have a maximum effect on the areas close to the wire. However, due to Brownian motions of fluid and temperature variations and magnetic field effects, this novel design can be observed in other regions. And finally, the effect of the new design on the amount of heat transfer, the temperature of the wire heater, and the CHF could be studied. To reach this goal, a pair of Helmholtz coils are designed and used to generate a homogenous alternating magnetic field around the wire heater.

2- Materials and methods

2- 1- Test equipment

To execute a series of pool boiling tests in steady-state conditions, a circuit like the one shown in Fig. 1a was designed. Fig. 1b depicts the actual image of the test circuit. For boiling studies, deionized water was utilized as the base fluid. To resist temperature variations caused by heat flux, boiling experiments were carried out in a Pyrex glass vessel. The boiling vessel was a cylinder with a diameter of 110 mm, a height of 300 mm, and a thickness of 3 mm. A round Plexiglass cap with an 8 mm thickness was employed to prevent the base fluid from evaporating out of the vessel. The copper electrodes on either side of the heater were held in place by the cap holes. A nickel-chrome (Cr20Ni30) wire with a diameter of 0.1 mm and a length of 70 *mm* was used as a heater. When DC[2] is delivered to both ends of a wire, ohmic resistance is formed along the wire, and some of the energy is dissipated as heat to the surrounding fluid, causing the boiling phenomenon. Two copper rods with a diameter of 12 *mm* and a length of 300 *mm* were used to provide electrical power on both ends of the wire heater with the least amount of power loss. These rods were covered with a varnished plastic coating to prevent oxidation and contamination of the boiling liquid. The wire heater is held horizontally and stretched using two steel clamps attached to the ends of each of these two rods. Part of the fluid that was evaporated due to the heat flux, was added to the boiling vessel to keep the control volume of the boiling constant. This was accomplished by using a cooling system that consists of a Pyrex spiral glass condenser connected to a pump and cold-water tank by two clear plastic glass hoses. The experiments were carried out

1 Boiling Heat Transfer Coefficient

2 Direct Current

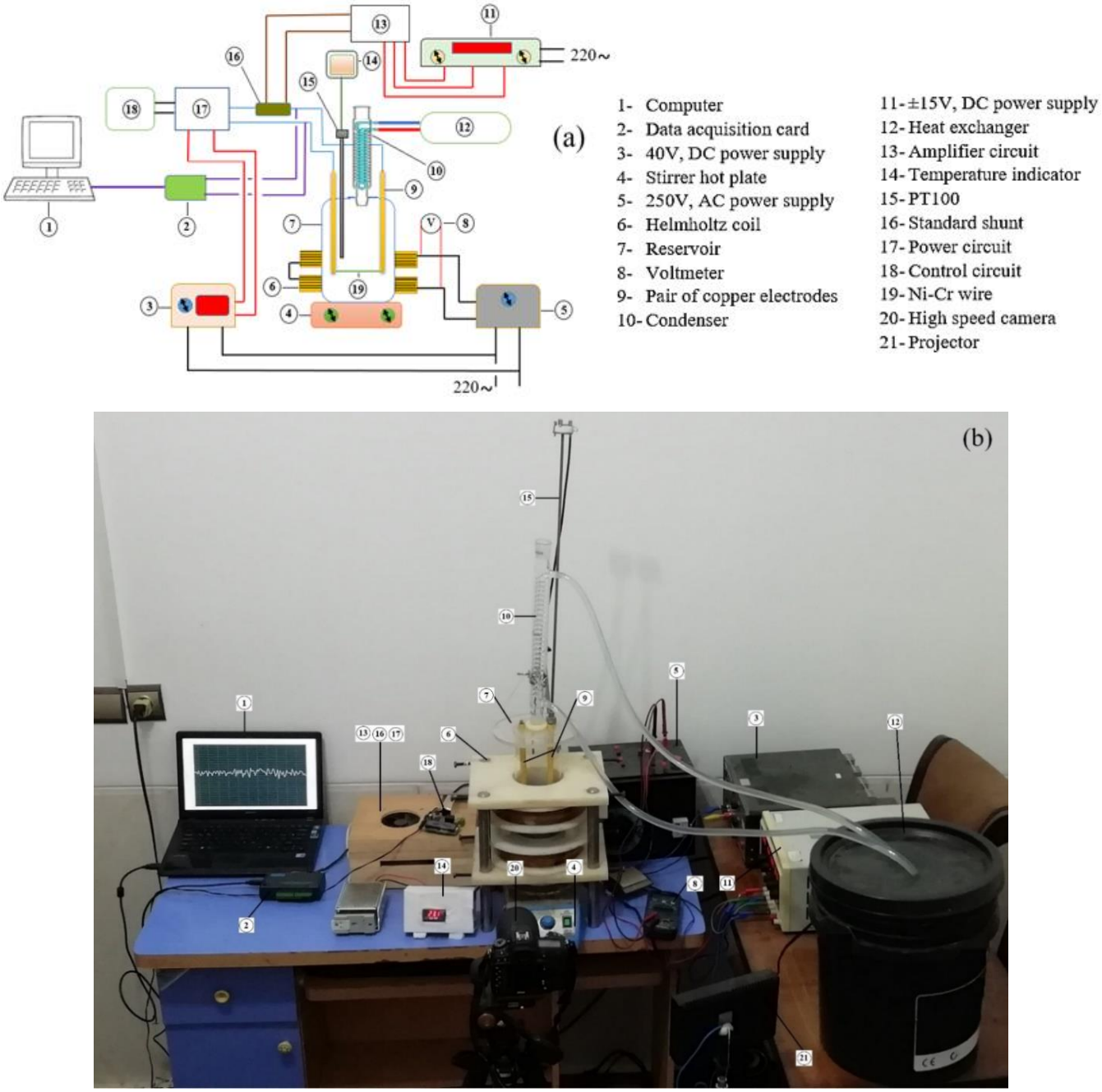

Fig. 1. (a) Schematic diagram of the pool boiling test circuit with alternating magnetic field application (b) The actual test circuit

under atmospheric pressure taking advantage of the open condenser.

During the experiments, it was critical to keep the working fluid at saturation temperature. This was done with a hot plate heater (model: ARE[1]) that can adjust the temperature range as well as the magnetic stirrer. An electronic controller was used to run experiments in steady-state conditions as it must be able to adjust the required electrical power to the wire heater. Three mainboards were constructed and used to apply a potential difference to the wire heater. A 40V DC power supply fed the power circuit, which transfers energy to the wire heater that converts electrical energy into heat flux (model: 405 HD[2]). A control circuit regulated how much electricity was applied to both ends of the heater. An amplifier circuit was used to set the voltage and amperage of both ends in the suitable range in order to electrically feed the control circuit. The voltage range applied to the amplifier circuit, which was ±15V, was also provided by a transformer with two independent DC outputs (model: APS3005S-3D[3]).

The mechanism of bubble formation or the physics governing the fluid around the wire heater should have been investigated for a more accurate analysis of the results. The experiments were recorded using 960 frames per second high-speed camera (model: RX10[4]) for this purpose.

According to the geometry of the boiling vessel, a magnetic field generator was designed and fabricated to apply an alternating magnetic field. The design was based on a pair of Helmholtz coils with a maximum magnetic field strength of 13.5mT. The coil pulleys were fabricated from Teflon materials to carry the weight of the wires without inducing magnetic flux. Fig. 2 depicts the schematic of a pair of Helmholtz coils. The strength of the magnetic field, B_x is calculated by:

$$B_x(x) = \frac{\mu_0 N I r^2}{2\left(x^2 + r^2\right)^{3/2}} \quad (1)$$

Adopted from [27]. In this equation, X represents the distance of the desired point on the central axis of the coils to the midpoint of the distance between the two coils, and r is the radius of each coil. μ_0, N and I are vacuum permeability constant, number of turns of coil and current intensity, respectively. Because the distance between the center of each coil and the midpoint of the distance between two coils (H) is equal to $r/2$ in the Helmholtz coils, the strength of the produced magnetic field is the same in both wires. Therefore, the total field strength at $r/2$ is:

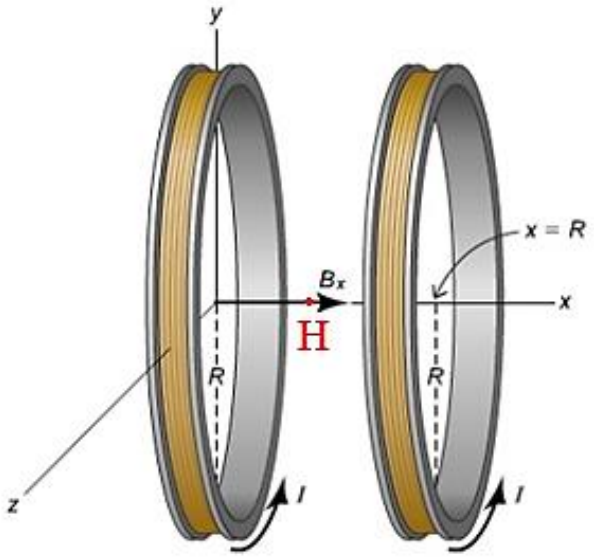

Fig. 2. Schematic of a pair of Helmholtz coils in the right-hand coordinate system

$$B_H\left(r/2\right) = 2B_x\left(r/2\right) = \frac{8}{5\sqrt{5}}\frac{\mu_0 N I}{r} \quad (2)$$

The magnetic field strength curve generated by the Helmholtz coils is shown in Fig. 3. Each coil creates a magnetic field around itself that is maximal at the center of the coil, as shown in this figure (green and red curves). When the coils are connected in series, the magnetic field generated in the space between them is approximately homogeneous and greater than the maximum value of each individual coil.

With optimization, the coil had an average diameter of 156 mm, a rectangular winding cross-section with dimensions of 46×40 mm, and an average distance between two coils of 100 mm. Also, the copper wire used for winding the cross-section of the coil had a diameter of one millimeter and was wrapped in 1450 turns on each coil. To minimize probable electrical leakage due to the coils' short circuit, a special thermal varnish was utilized between the layers.

To enhance this field, the magnetic field vector created in both coils must be in the same direction. To accomplish this, the two coils must be connected in series and connected to an AC power converter. The output voltage of an autotransformer with alternating output was adjustable from zero to 250 volts. The current intensity varies as the voltage changes due to the resistance of the coil windings, according to Ohm's law [28], and the strength of the generated magnetic field changes as well, according to Eq. (1). The apparatus used to generate an alternating magnetic field and measure its strength is depicted in Fig. 4. Before performing the main boiling test at the location of the wire heater (on the axis that runs through the

1 Manufacture: VELP
2 Manufacture: Eram Electronic
3 Manufacture: ATTEN
4 Manufacture: SONY

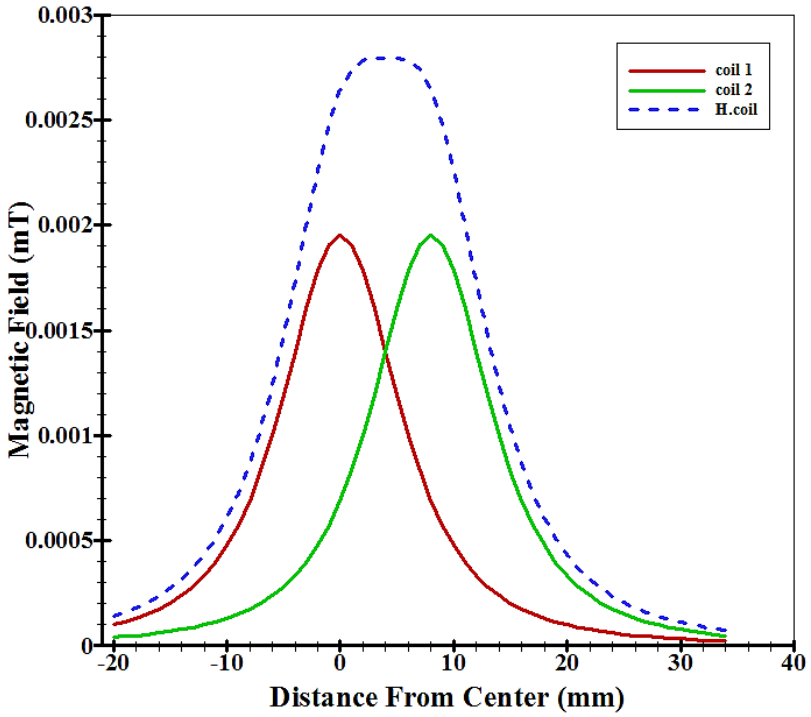

Fig. 3. Magnetic field intensity resulting from the connection of Helmholtz coils in a series mode in the middle of the distance between two coils and on the axis passing through each center

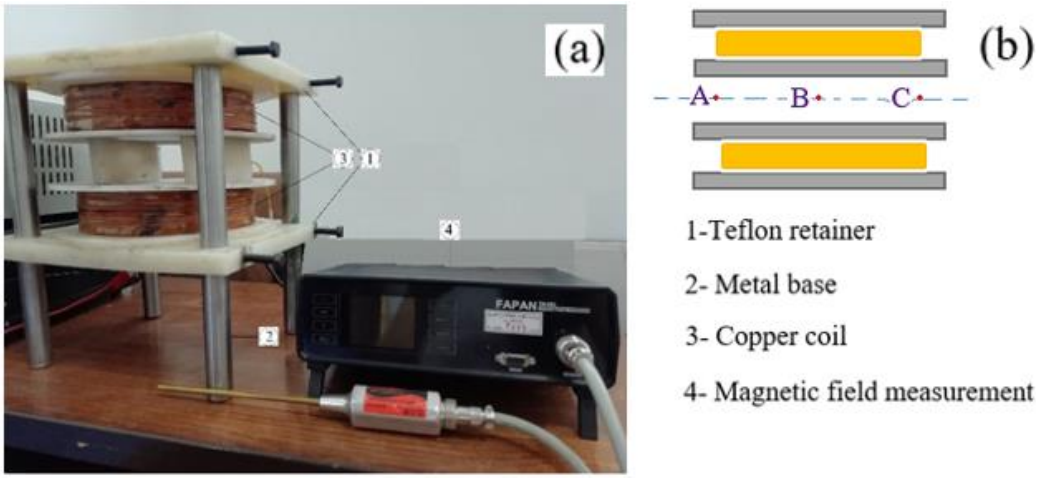

Fig. 4. (a) Equipment for the generation and measurement of alternating magnetic fields with different intensities (b) Measurement of the intensity of the generated magnetic field in different parts of the Helmholtz coil, A and C (coil edges), B (coil center)

Table 1. The intensity of the generated magnetic field at different points of the Helmholtz coil measured before the experiments.

~	Magnetic Field (mT)		
	C	**B**	**A**
100 V	5.9	5.8	5.9
125 V	7.5	7.3	7.5
150 V	9.1	8.9	9.1
190 V	11.6	11.3	11.6
225 V	13.5	13.3	13.5

middle of the distance between the two coils), the magnetic field intensity was measured using the magnetic field intensity measuring device[1] at three points: A and C (the coil's edges), point B (the coil center). Table 1 shows the measured values of magnetic field intensity in these three points. The magnetic field intensity values produced according to this table have been obtained by applying voltages of 100 V, 125 V, 150 V, 190 V, and 225 V.

2- 2- Test method

The heat flux in the wire heater was generated in the form of ramp-wise in the steady-state conditions during the pool boiling experiments. As a result, the current passing through the heater increases as the electrical potential difference between the two ends of the wire heater increases by $\Delta V = 1\ \mathrm{V}$. The waiting time to increase voltage was roughly 5 minutes to attain stable circumstances. After that time, the voltage and current fluctuations were monitored to be negligible to keep the wire heater temperature constant. As a result, Eq. (3) may be used to assume that the heater's average power output is constant:

$$\bar{q} = \bar{I} \times \Delta\bar{V} \tag{3}$$

To calculate the heat flux delivered to the fluid at each time step, it must be considered that a portion of the total energy is stored in the wire heater as sensible heat, and the remainder is transferred to the surrounding liquid. The first law of thermodynamics is as follows:

$$\Delta\bar{U} = \bar{E}_{in} - \bar{E}_{out} \tag{4}$$

Where $\bar{E}_{in}$ is the input electrical energy to the wire heater (here $(-(\bar{q}''))$), $\Delta\bar{U}$ represents the average internal energy change (sensible heat) stored in the heater ($mC_p \frac{dT_w}{dt}$) and $\bar{E}_{out}$ is the heat energy delivers to the working fluid. The average wall superheats temperature is $\Delta\bar{T}_w = \bar{T}_w - T_{sat}$, where, $\bar{T}_w$ and T_{sat} are heater temperature and saturation temperature, respectively. It can be calculated by:

$$\Delta T_w = \frac{R - R_0}{\alpha R_0} \tag{5}$$

Adopted from [29]. Where R_0 is the initial resistance of the wire heater at the boiling fluid's saturation temperature, α is the resistance-temperature coefficient of the wire heater measured to be 0.0041/°C for this alloy. R can also be calculated by ohm's law[28]. Now the wire heater energy $\bar{q}''$ can be calculated by:

$$\bar{q}'' = \frac{1}{A_{ht}}\left[\bar{I} \times \Delta\bar{V} - \rho v C_p \frac{\Delta\bar{T}_w}{\Delta t}\right] \tag{6}$$

In this case, v is the heater's volume, A_{ht} is the heat transfer surface, ρ is the density, and C_p is the heater's specific heat capacity. Because the temperature derivative to time is zero in steady-state conditions, the second term of Eq. (6) is zero, and the average heat flux to the working fluid equals:

$$\bar{q}'' = \frac{1}{A_{ht}}\left[\bar{I} \times \Delta\bar{V}\right] \tag{7}$$

By calculating the heat flux in each stage of the boiling

1 Manufacture: FAPAN

experiment and using Eq. (4) to calculate the temperature of the wire heater, the heat transfer coefficient (***h***) can be computed using the following equation:

$$h = \frac{q''}{\Delta \bar{T}_w} \tag{8}$$

In a set of steady-state boiling experiments, three strengths of alternating magnetic fields with values (5.8, 8.9, 13.3 mT) were generated by applying voltages (100, 150, 225V), and their influence on the boiling phenomena was investigated.

2- 3- Uncertainty analysis

When measuring a parameter, several factors such as the measuring device's precision, operator error, environmental conditions, and geometry can all affect the precision of the measurement, generally referred to as measurement errors. Thus even with the highest level of measurement precision and the most accurate methodologies, the measured values are affected by inevitable uncertainties. Statistical analyses were performed on a set of measurement data to quantify such uncertainties. The Moffat technique [30] is one of the most extensively used methods to perform uncertainty analysis. According to this method, if the variable ***R*** is a function of measured values of an independent variable $\boldsymbol{X_i}$ – i.e, $R\left(X_1, X_2, \ldots X_N\right)$, the δR uncertainty can be calculated by:

$$\delta R = \left\{ \sum_{i=0}^{N} \left(\frac{\partial R}{\partial X_i} \delta X_i \right)^2 \right\}^{1/2} \tag{9}$$

The uncertainty relationships of wire heater area, current, heater volume, heater temperature, heat flux, and boiling heat transfer coefficient were calculated by following equations:

$$\frac{U_A}{A} = \sqrt{\left(\frac{U_r}{r}\right)^2 + \left(\frac{U_L}{L}\right)^2} \tag{10}$$

$$\frac{U_I}{I} = \sqrt{\left(\frac{U_{\Delta V_{shunt}}}{\Delta V_{shunt}}\right)^2 + \left(\frac{U_{R_{shunt}}}{R_{shunt}}\right)^2} \tag{11}$$

$$\frac{U_I}{I} = \sqrt{\left(\frac{U_{\Delta V_{shunt}}}{\Delta V_{shunt}}\right)^2 + \left(\frac{U_{R_{shunt}}}{R_{shunt}}\right)^2} \tag{12}$$

$$\frac{U_I}{I} = \sqrt{\left(\frac{U_{\Delta V_{shunt}}}{\Delta V_{shunt}}\right)^2 + \left(\frac{U_{R_{shunt}}}{R_{shunt}}\right)^2} \tag{13}$$

$$\frac{U_{q''}}{q''} = \sqrt{\left(\frac{U_A}{A}\right)^2 + \left(\frac{U_I}{I}\right)^2 + \left(\frac{U_{\Delta V_h}}{\Delta V_h}\right)^2} \tag{14}$$

$$\frac{U_H}{H} = \sqrt{\left(\frac{U_{q''}}{q''}\right)^2 + \left(\frac{U_{T_w}}{T_w}\right)^2} \tag{15}$$

In Eqs. (10) to (15), ***U*** represent uncertainty, ***A***, ***r*** and ***L*** represent surface, radius and length of heater, respectively, ***I*** and $\Delta \boldsymbol{V_h}$ represent current and potential difference of the wire heater, $\Delta \boldsymbol{V_{shunt}}$ and $\boldsymbol{R_{shunt}}$ represent potential difference and ohmic resistance of shunt. The computed uncertainties using the above relations and the results obtained from all experiments are shown in Table 2.

Table 2. Calculated uncertainties of equipment and effective parameters in pool boiling

	wire heater area	current	heater volume	heater temperature	heat flux	boiling heat transfer coefficient
Uncertainty (%)	1.23	2.26	2.12	2.26	4.03	4.62

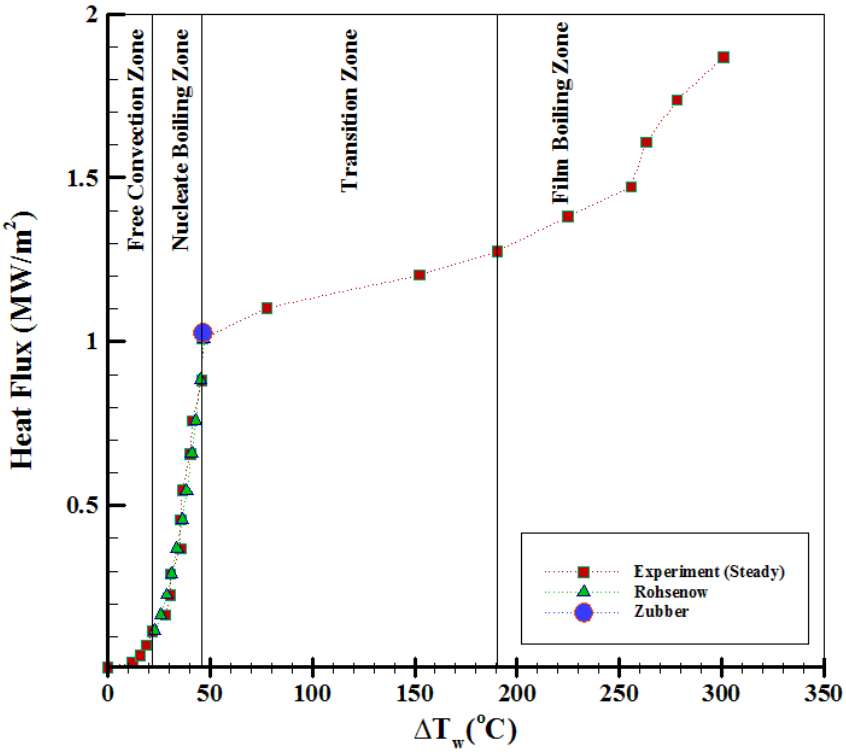

Fig. 5. Pool boiling of saturated deionized water under atmospheric pressure in steady conditions and is compared to the correlations of Rohsenow [31] and Zuber [32].

3- Results and discussion

3- 1- Test validation

First, we examined the validity of the results in comparison with reference correlations. Fig. 5 depicts a pool boiling diagram of saturated deionized water around a wire heater under atmospheric pressure. For the steady-state boiling of deionized water, the experimental results were compared to Rohsenow [31] and Zuber correlations [32] to the red line and blue dot, respectively. The both studies correlations were employed to validate the nucleate boiling region and CHF value, as expressed in the following equations:

$$\Delta T_w = {C_{sf}}/{C_p}\,.h_{fg}\left[\frac{q''}{\mu.h_{fg}}\sqrt{\frac{\sigma}{g\left(\rho_l-\rho_g\right)}}\right]^{.33}.\left(\frac{C_p.\mu}{k}\right)^n \quad (16)$$

$$q''_{CHF} = 0.131\times h_{fg}\times\left(g\sigma\left(\rho_l-\rho_v\right)\right)^{1/4} \quad (17)$$

Where the coefficients C_{sf} and $\boldsymbol{n}$ are determined by experience and depend on the surface conditions and the type of fluid being boiled [33]. For nickel-chromium wire, these factors are 0.0062 and 0.49, respectively $C_p, h_{fg}, \sigma, \rho, \mu$. and $\boldsymbol{k}$ are specific heat, latent heat of vaporization, surface tension coefficient, density, dynamic viscosity and thermal conductivity of water at saturation temperature, respectively.

To ensure the obtained results, this experiment has been repeated three times. Table 3 shows the results related to the critical heat flux in steady-state conditions. As can be seen in the last two columns, the amount of difference in each case is within the engineering error and can confirm the steady-state boiling conditions to an acceptable extent. According to the results of this table, the third experiment showed less error and was selected for validation. As shown in Fig. 5, the obtained results in the nucleate boiling zone, are in good agreement with the Rohsenow and Zuber relationship.

Fig. 5 also shows that all boiling regimes can be displayed separately in this diagram. Free convection flows cause the fluid to move near the heating surface in the free convection boiling regime. The fluid near the heater's surface is at saturation temperature and evaporates when it comes into contact with the surface by receiving additional heat. The slope of the boiling curve dramatically increases after the free convection phase ends and nucleate boiling begins. In this regime, tiny bubbles form and disperse into the liquid after detaching from the surface. As the temperature rises, bubbles expand more quickly and rise to the liquid's surface, where they disperse. Bubbles are formed in the nucleate boiling region by the expansion of trapped gas or vapor in small cavities on the surface. Bubbles grow up to a specific

Table 3. The deviation values of q''_{CHF} from the values obtained by Rohsenow and Zuber correlations in the boiling curve of deionized water under steady-state conditions

Test NO.	CHF (MW/m^2)	Wall Superheated Temperature in CHF	Difference in value with Zuber correlation (%)	Difference in value with Rohsenow correlation (%)
1	1.0442	48.54	1.57	3.6
2	0.9673	43.2	5.9	4.2
3	1.0078	46.36	1.96	0.1

size based on surface tension at the liquid-vapor interface, temperature, and pressure. Depending on the superheated temperature, the generated bubbles may collapse on the surface, expand and separate from the surface to disseminate throughout the liquid volume, or reach the liquid surface at sufficiently high temperatures before bursting[34]. There are two causes for the high heat transmission in this regime[35] First, the upward migration of the bubbles generates a vigorous stirring of the liquid around the heater's surface, transferring heat more quickly to the liquid's body. Second, vapor bubbles (which have a higher energy level than liquids) release their trapped energy in the liquid when they move toward the liquid surface (due to buoyancy) and burst in the liquid domain.

Bubbles form so quickly once the nucleate boiling regime ends, thus they cover the heating surface and form a vapour layer and prevent operating fluid (water) to access the heating surface directly. The heat in this region must pass through the vapour layer by conduction to reach the liquid. This film's thermal resistance lowers heat transfer into the operating fluid (water) and causes some sections underneath the vapour layer to overheat. The zone after nucleate boiling is referred to as the transition regime, which is unstable and when it ends, a stable film boiling is created by connecting the bubble layers around the wire heater, resulting in an isolated region surrounding the heater's surface. As a result, it significantly prevents the heat transfer from the heater to the liquid, causing the wire temperature to rise excessively, as the wire turns red and gleams. Heat transmission during the film boiling regime is most likely by a radiation mechanism[36].

A high-speed camera was used to obtain high-quality and accurate images of the various stages of boiling. The obtained images show the different boiling regimes, the behavior of the bubbles in each stage, and the vapor film. Also, by using these images, the conditions of the heater can be seen at each stage of boiling. According to the images shown in Fig. 6, when the heat flux is $19.3\,KW/m^2$, no bubbles are observed. This stage is the beginning of free convection boiling. By increasing the heat flux to $23\,KW/m^2$, the images show the beginning of nucleate boiling. At this stage, bubbles start to form from both ends of the heater and separate from the surface. In

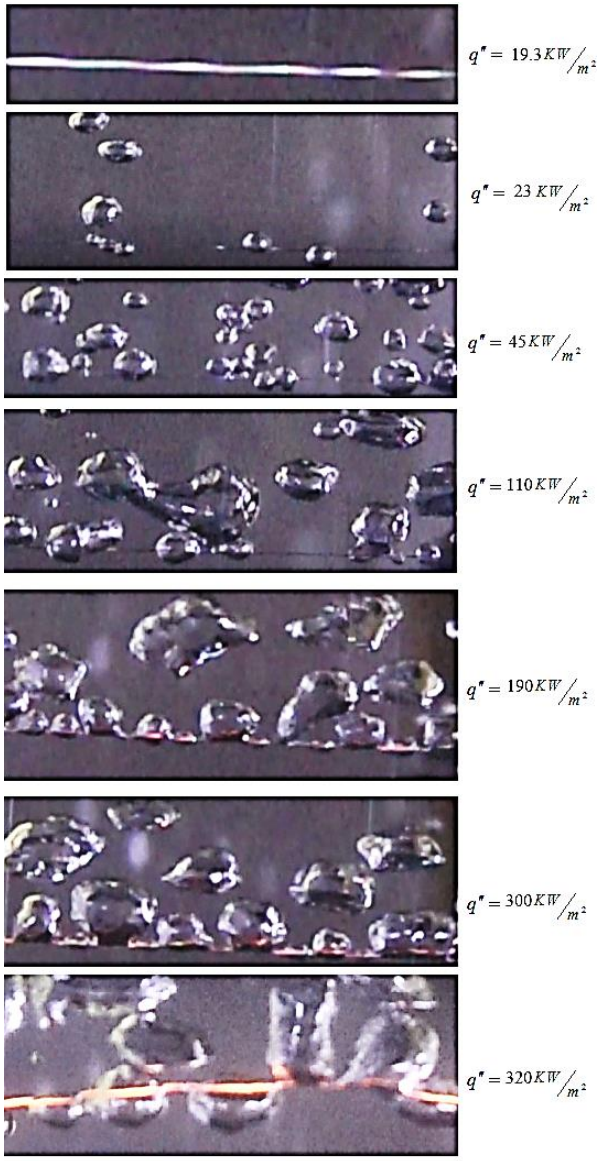

Fig. 6. Images of bubbles formed during different boiling regimes around the heater wire

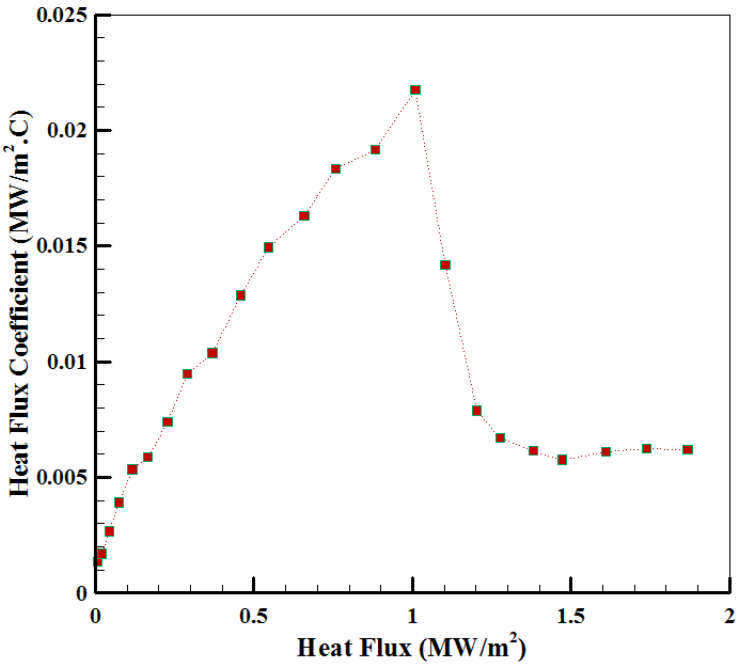

Fig. 7. Changes in heat transfer coefficient in all pool boiling regimes of saturated deionized water under atmospheric pressure and steady conditions

this regime, the more the boiling is in the initial stages, the more bubbles (which are not visible) cover the surface of the wire heater in the form of a micro-layer in some longitudinal points of the wire heater [37]. At 45 KW/m^2, the bubbles cover the entire heater, and the rate of bubble generation increases in nucleate boiling. These bubbles merge at the top of the heater. At 110 KW/m^2, the size of the separated bubbles becomes larger and the length of the heater increases slowly due to the high temperature. At this stage, coalescence of larger bubbles at the top of the heater is reduced. At 190 KW/m^2, the boiling enters the film boiling stage. At this stage, the bubbles separated from the surface become larger and merge near the surface of the heater. Also, some points of the heater turn red. With the increase of the heat flux, at 300 KW/m^2, the bubbles cover the entire surface in the form of films and irregular shapes with a lower production frequency. Also, due to the high heat flux, the temperature of the heater rises sharply. In this case, the entire surface of the wire becomes shiny red and due to the increase in buoyancy force, the increased length of the wire is stretched upward. Finally, during the film boiling regime, the wire heater melts at a point with the least mechanical resistance (panel (**e**)). At this point, the boiling process stops.

Fig. 7 shows the boiling heat transfer coefficient as a function of the heat flux. In this diagram, in the free-convection boiling zone, where the rate of temperature change and heat flux is low, the heat transfer coefficient increases with a slight slope. However, in the nucleate boiling zone, where the rate of increase of heat flux is high and the changes in wall superheated temperature are low, the heat transfer coefficient increases steeply. Although the heat flux provided to the fluid increases slightly in the transition regime, due to the formation of a bubble film around the wire heater, which functions as a layer of thermal resistance, the wall superheated temperature rises dramatically. Hence, the heat transfer coefficient is reduced as a result of this increment. Then, in the first part of the film boiling regime, the mushroom bubbles which are formed by bubble adhesion, are separated from the heater's surface, and moved towards the liquid surface. The rate of increase of wall superheated temperature relative to the transition regime decreases slightly and the heat transfer coefficient increases slightly. Bubbles that cover the entire volume around the heater, prevent the surface of the heater from coming into contact with the liquid in the second part of the film boiling, causing the wire heater's temperature to rise too much by forming a layer of thermal resistance. This state persists until the wire heater's resistance is lost and it breaks. The heat transfer coefficient is decreased in this region.

3- 2- Boiling of deionized water under the influence of an alternating magnetic field

To investigate the effect of an alternating magnetic field on boiling basic parameters, alternating magnetic fields of 5.8, 8.9, and 13.3 mT with a frequency of 50Hz were produced by applying voltages of 100, 150, and 225V to the built Helmholtz coils, respectively. The corresponding fields are homogeneous in the middle of the distance between the two coils and in the longitudinal direction of the heater,

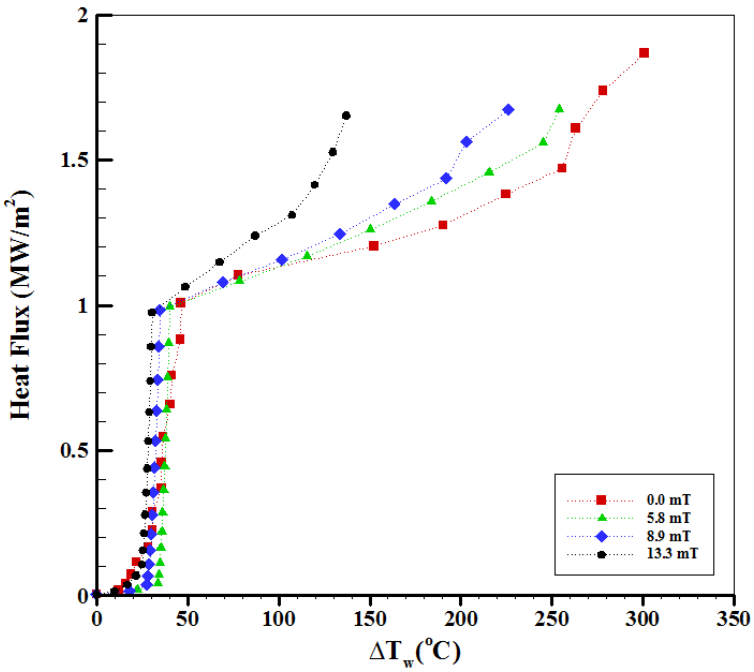

Fig. 8. Comparison of pool boiling diagrams of saturated deionized water under atmospheric pressure and steady conditions at different magnetic field intensities

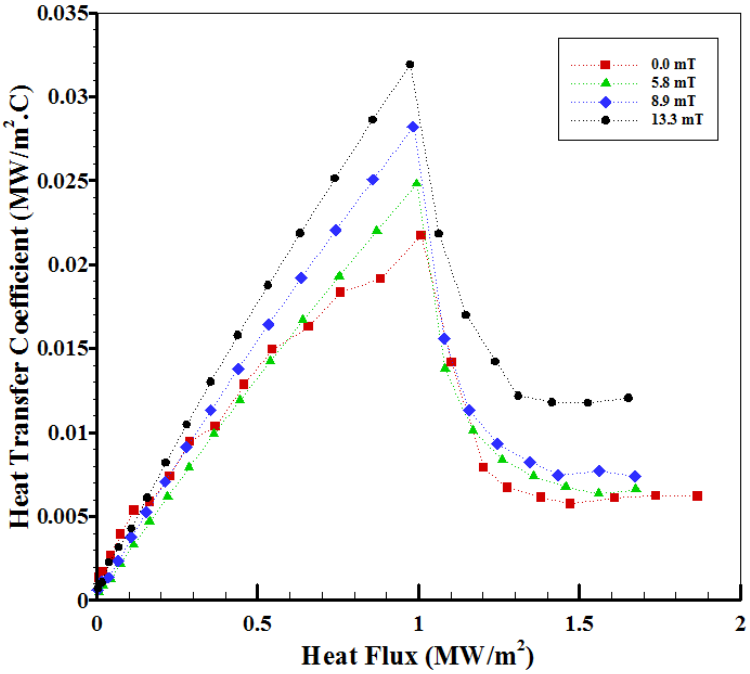

Fig. 9. Comparison of pool boiling diagrams of saturated deionized water under atmospheric pressure and omparison of pool boiling heat transfer coefficient diagrams of saturated deionized water under atmospheric pressure and steady conditions at different magnetic field intensities

according to Eq. (2) and Fig. 3. Fig. 8 depicts the steady-state boiling curves of deionized water, and Fig. 9 depicts the results of variations in the corresponding heat transfer coefficient under the application of three different intensities of magnetic field versus non-application of magnetic field circumstances. The findings reveal that in the early stages of boiling, the application of an alternating magnetic field reduces the active sites of nucleation on the surface of the heater and delays ONB. Also, it speeds up the shift of the boiling process from this region to the transition phase. The

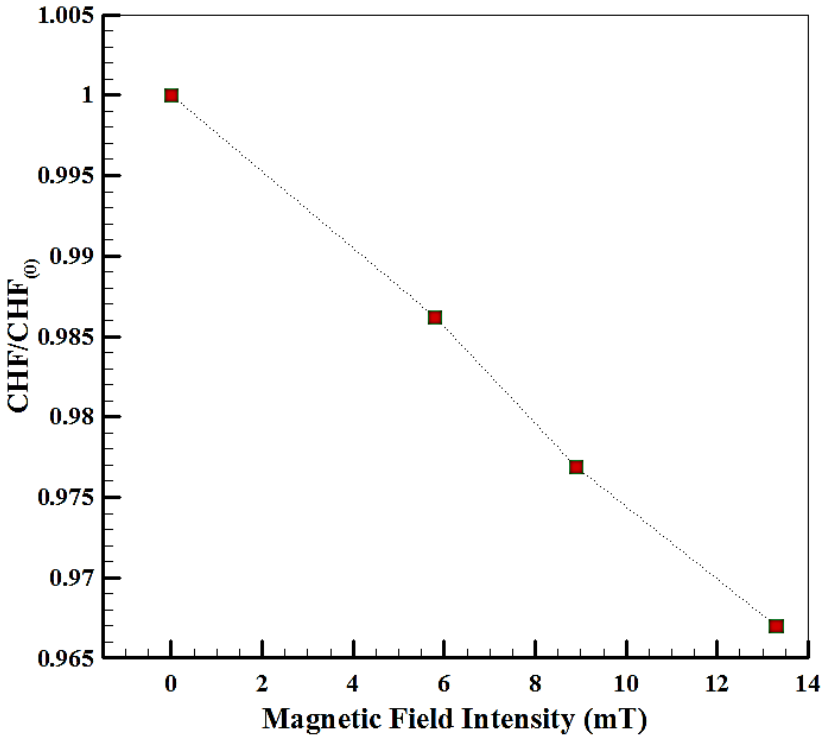

Fig. 10. Dimensionless CHF changes in the pool boiling of saturated deionized water under atmospheric pressure and steady conditions at different magnetic field intensities

slope of the boiling curve in all boiling regimes is greater in the presence of a magnetic field than in the absence of one, according to the results of Fig. 8. According to research [38], the higher slope can be due to the increase in the necessary heat flux at the corresponding superheated temperature, which is caused by the increase in viscosity, surface tension and enthalpy of magnetized water. Due to the influence of magnetic body forces, the void fraction of the bubbles decreases with increasing magnetic field intensity in two-phase flow [18]. An alternating magnetic field ionizes water molecules, making them behave like charged particles. The presence of this type of magnetic field with an intensity of $\boldsymbol{B}$ around the wire heater causes Lorentz's force [39] to be applied to the ionized water molecules around the surface of the heater:

$$F = QuB \times Sin\,\theta \tag{18}$$

Where the angle between the charged particle's velocity vector and the magnetic field's vector in this relationship is θ , $\boldsymbol{u}$ is the velocity of charged particles with a magnitude of $\boldsymbol{Q}$, and $\boldsymbol{B}$ is the strength of the applied magnetic field.

Another reason for the increase in heat transfer in boiling regimes due to the use of an alternating magnetic field is that the presence of frequency in the alternating current causes the direction of the generated magnetic field to change alternately. As a result, the direction of the Lorentz force exerted on the fluid's ionized molecules alternatively changes and their movement inside the vessel accelerates. As a result, the heat transfer coefficient increases. Additionally, based on the findings in Fig. 8, the boiling regimes cease quicker than typical as the magnetic field's intensity increases. Reducing the number of bubbles around the wire heater causes the heat generated in the heater to be transferred more quickly to the surrounding liquid. As a result, the wall superheated temperature decreases as the magnetic field intensity increases. Due to the change of direction depending on the frequency of Lorentz force applied to water molecules around the wire heater, low amplitude and high-frequency vibrations were observed along the length of the wire. The presence of irregular vibrations along the length of the wire caused the wire to get fatigued and break earlier than usual. The results showed that the higher the intensity of the applied magnetic field, due to the increase in the frequency of vibrations, the wire heater broke at a lower temperature and the boiling ended. As the overall superheated temperature drops, so does the heat transfer coefficient, which is inversely related to this parameter. Compared to liquid molecules, bubbles have less capacity to absorb excess heat. The increase in the movement of the bubbles with the increase in the intensity of the magnetic

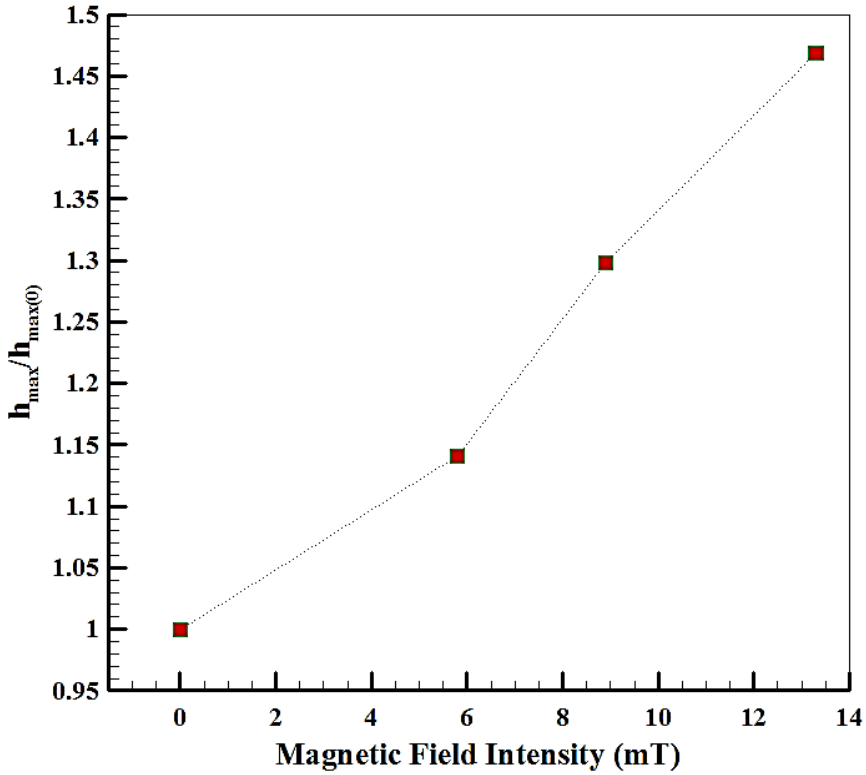

Fig. 11. Dimensionless heat transfer coefficient changes at CHF point in the pool boiling of saturated deionized water under atmospheric pressure and steady conditions at different magnetic field intensities

field causes an increase in their collision with each other and as a result the formation of larger bubbles. Therefore, the capacity to receive more heat in the nucleate boiling regime is reduced and as a result, CHF is reduced. Figs. 10 and 11 depict the dimensionless CHF and heat transfer coefficient alterations caused by the application of alternating magnetic fields, respectively. In these diagrams, (0) refers to the state without applying a magnetic field.

According to the results, the rate of CHF reduction is 1.38%, 2.31%, and 3.33%, respectively, if magnetic fields of 5.8, 8.9, and 13.3 mT were applied. The greatest changes in boiling heat transfer coefficient are related to the CHF point. At intensities of 5.8, 8.9, and 13.3 mT, the rate of increase of this coefficient is 14%, 30%, and 47% respectively, at the CHF point.

4- Conclusion

Pool boiling heat transfer and CHF were studied in steady-state conditions under the application of an alternating magnetic field with a frequency of 50Hz and various intensities experimentally. A horizontal nickel-chrome wire was used as a heater. To apply heat flux to the heater in each stage of the experiment, the voltage was increased by one volt. Deionized water's boiling curve in the nucleate boiling regime was compared with Rohsenow and Zuber correlations to confirm the validity of the experiment's findings. The findings demonstrate that the acquired values are in good agreement with these correlations. The quantity of heat flux achieved at the CHF point deviating by only 0.1% and 2% from Rohsenow's and Zuber's correlations, respectively.

To investigate the role of an alternating magnetic field on the pool boiling process, a homogeneous magnetic field in the space between the two coils and in a radial direction was created by building a pair of copper coils and application of AC. The results demonstrated that applying a magnetic field increases the ONB and accelerates transfer from the nucleate boiling regime to the transition boiling regime. The overall time of the pool boiling process also decreased with increasing magnetic field intensity. The CHF was reduced by 1.38%, 2.31%, and 3.33%, respectively, when magnetic field strengths of 5.8, 8.9, and 13.3 mT were applied, compared to when the magnetic field was not applied. In all regimes, the effect of applying an alternating magnetic field on the variation of the boiling heat transfer coefficient is obvious. The maximum rate of this coefficient's increment was 14%, 30%, and 47% for magnetic field strengths of 5.8, 8.9, and 13.3mT, respectively, at the CHF point. In general, using an alternating magnetic field has little effect on CHF, but it enhances boiling's overall heat transfer coefficient.

Nomenclature

A	Heater surface (m^2)
B	Magnetic field strength (T)
C_p	Specific heat capacity (J/Kg.K)
dt	Time difference (s)
$\bar{E}$	Average energy (W/m^2)
F	Lorentz force (N)
g	Gravity acceleration (m/s^2)
H	Heat transfer coefficient ($W/m^2.C$)
h_{fg}	Fluid's latent heat (Kj/Kg)
I	Current intensity (A)
N	Number of turns of coil
Q	Charge (coulomb)
q	Heat flux (W/m^2)
R	Ohmic resistance (Ω)
r	Coil radius (m)
U	Velocity (m/s)
V	Voltage (v)
v	Heater volume (m^3)
x	Distance from center of Helmholtz coil(m)
x_i	Independent variable

Greek symbols

α	resistance-temperature coefficient (1/°C)
$\delta R, U$	uncertainty
$\Delta\bar{T}_w$	wire superheat temperature ($=\bar{T}_w - T_{sat}$,°C)
$\Delta\bar{U}$	average internal energy change (W/m^2)
$\Delta\bar{V}$	average potential drop (v)
θ	angle (Deg)
μ	dynamic viscosity (Kg/m.s)
μ_0	vacuum permeability constant $= 4\pi \times 10^{-7}$ N/A^2
ρ	density (Kg/m^3)
σ	surface tension (N/m)

Subscript

ht	heater
t	time (s)
0	reference point
CHF	critical heat flux (W/m^2)
g	gas
in	input
l	liquid
out	output

Superscript

-	average
$''$	per unit area ($1/m^2$)

References

[1] X.-F. Pang, B. Deng, The changes of macroscopic features and microscopic structures of water under influence of magnetic field, Physica B: Condensed Matter, 403(19) (2008) 3571-3577.

[2] S. Alangar, Effect of boiling surface vibration on heat transfer, Heat and Mass Transfer, 53(1) (2017) 73-79.

[3] T.-B. Chang, Z.-L. Wang, Experimental investigation into effects of ultrasonic vibration on pool boiling heat transfer performance of horizontal low-finned U-tube in TiO2/R141b nanofluid, Heat and Mass Transfer, 52(11) (2016) 2381-2390.

[4] H.J. Kim, J.H. Jeong, Numerical Analysis of Experimental Observations for Heat Transfer Augmentation by Ultrasonic Vibration, Heat Transfer Engineering, 27(2) (2006) 14-22.

[5] K.F. Jongdoc Park, Qiusheng Liu, Critical heat flux phenomena depending on pre-pressurization in transient heat input, in: AIP, 2017, pp. 080005.

[6] Y. Li, K. Fukuda, Q. Liu, Steady and Transient CHF in Subcooled Pool Boiling of Water under Sub-atmospheric Pressures, Marine Engineering, 52(2) (2017) 245-250.

[7] H. Moghadasi, H. Fathalizadeh, A. Mehdikhani, H. Saffari, Surface Modification Utilizing Photolithography Process for Pool Boiling Enhancement: An Experimental Study, Heat Transfer Engineering, 43(12) (2022) 1008-1024.

[8] M. Shojaeian, M. Yildizhan, Ö. Coşkun, E. Ozkalay, Y. Tekşen, M. Gulgun, H. Acar, A. Kosar, Investigation of change in surface morphology of heated surfaces upon pool boiling of magnetic fluids under magnetic actuation, Materials Research Express, 3 (2016) 096102.

[9] A. Walunj, S. Alangar, Experimental Investigation on Transient Pool Boiling Heat Transfer from Rough Surface and Heat Transfer Correlations, International Journal of Heat and Technology, 37 (2019) 545-554.

[10] A. Walunj, A. Sathyabhama, Transient CHF enhancement in high pressure pool boiling on rough surface, Chemical Engineering and Processing - Process Intensification, 127 (2018) 145-158.

[11] A. Ayoobi, A.F. Khorasani, M. Ramezanizadeh, A. Afshari, Experimental investigation of transient pool boiling characteristics of Fe3O4 ferrofluid in comparison with deionized water, Applied Thermal Engineering, 179 (2020) 115642.

[12] L. Cheng, G. Xia, Q. Li, J. Thome, Fundamental Issues, Technology Development And Challenges Of Boiling Heat Transfer, Critical Heat Flux And Two-Phase Flow Phenomena With Nanofluids, Heat Transfer Engineering, 40 (2018).

[13] L. Fan, J. Li, D.-Y. Li, L. Zhang, Z.-T. Yu, K.-F. Cen, The effect of concentration on transient pool boiling heat transfer of graphene-based aqueous nanofluids, International Journal of Thermal Sciences, 91 (2015).

[14] M. Mohammadpourfard, H. Aminfar, M. Sahraro, Numerical simulation of nucleate pool boiling on the

horizontal surface for ferrofluid under the effect of non-uniform magnetic field, Heat and Mass Transfer, 50(8) (2014) 1167-1176.
[15] P. Naphon, Effect of Magnetic Fields on the Boiling Heat Transfer Characteristics of Nanofluids, International Journal of Thermophysics, 36(10) (2015) 2810-2819.
[16] J. Ishimoto, M. Okubo, S. Kamiyama, M. Higashitani, Bubble Behavior in Magnetic Fluid under a Nonuniform Magnetic Field, JSME International Journal Series B, 38(3) (1995) 382-387.
[17] S.-D.O.H.-Y. Kwak, A Study of Bubble Behavior and Boiling Heat Transfer Enhancement under Electric Field, Heat Transfer Engineering, 21(4) (2000) 33-45.
[18] P.S. Lykoudis, Bubble growth in the presence of a magnetic field, International Journal of Heat and Mass Transfer, 19(12) (1976) 1357-1362.
[19] L. Hołysz, A. Szcześ, E. Chibowski, Effects of static magnetic field on water and electrolyte solutions, Journal of colloid and interface science, 316 (2008) 996-1002.
[20] H. Habibi Khoshmehr, A. Saboonchi, M.B. Shafii, N. Jahani, The study of magnetic field implementation on cylinder quenched in boiling ferro-fluid, Applied Thermal Engineering, 64(1) (2014) 331-338.
[21] A.H. Mahmoudi, E. Abu-Nada, Combined Effect of Magnetic Field and Nanofluid Variable Properties on Heat Transfer Enhancement in Natural Convection, Numerical Heat Transfer, Part A: Applications, 63(6) (2013) 452-472.
[22] A. Abdollahi, M.R. Salimpour, N. Etesami, Experimental analysis of magnetic field effect on the pool boiling heat transfer of a ferrofluid, Applied Thermal Engineering, 111 (2016).
[23] A.R. Ayoobi, A.R. Faghih Khorasani, Study of transient pool boiling of deionized water in two modes of presence and absence of a magnetic field, Journal of Solid and Fluid Mechanics, 10(1) (2020) 209-221.
[24] P. S.LYKOUDIS, Bubble growth in the presence of a magnetic field, Heat and Mass Transfer, 19 (1976) 1357-1362.
[25] A. Vatani, P. Woodfield, N.-T. Nguyen, D.V. Dao, Thermomagnetic Convection Around a Current-Carrying Wire in Ferrofluid, Journal of Heat Transfer, 139 (2017).
[26] Q. Li, Y. Xuan, Experimental investigation on heat transfer characteristics of magnetic fluid flow around a fine wire under the influence of an external magnetic field, Experimental Thermal and Fluid Science, 33(4) (2009) 591-596.
[27] W.M. Frix, G.G. Karady, B.A. Venetz, Comparison of calibration systems for magnetic field measurement equipment, IEEE Transactions on Power Delivery, 9(1) (1994) 100-108.
[28] T. Henry, Ohm's Law, Electrical Math and Voltage Drop Calculations, Henry Publications, 1992.
[29] L. Weiner, P. Chiotti, H.A. Wilhelm, U.S.A.E. Commission, A. Laboratory, Temperature Dependence of Electrical Resistivity of Metals, United States Atomic Energy Commission, Technical Information Service, 1952.
[30] R.J. Moffat, Describing the uncertainties in experimental results, Experimental Thermal and Fluid Science, 1(1) (1988) 3-17.
[31] M. Yaghoubi, K. Hirbodi, M.R. Nematollahi, S. Bashiri, Experimental Study of Subcooled Pool Boiling around a Circular Rough Cylinder, AUT Journal of Mechanical Engineering, 1(1) (2017) 21-28.
[32] N. Zuber, Nucleate boiling. The region of isolated bubbles and the similarity with natural convection, International Journal of Heat and Mass Transfer, 6(1) (1963) 53-78.
[33] I. Pioro, Experimental Evaluation of Constants for the Rohsenow Pool Boiling Correlation, International Journal of Heat and Mass Transfer, 42 (1998) 2003-2013.
[34] J.P. Holman, Heat Transfer, McGraw-Hill, 2002.
[35] M. Joyce, Chapter 7 - Cooling and Thermal Concepts, in: M. Joyce (Ed.) Nuclear Engineering, Butterworth-Heinemann, 2018, pp. 129-166.
[36] A. Sakurai, M. Shiotsu, K. Hata, A General Correlation for Pool Film Boiling Heat Transfer From a Horizontal Cylinder to Subcooled Liquid: Part 2—Experimental Data for Various Liquids and Its Correlation, Journal of Heat Transfer, 112(2) (1990) 441-450.
[37] Y.-H. Zhao, T. Masuoka, T. Tsuruta, Theoretical studies on transient pool boiling based on microlayer model, International Journal of Heat and Mass Transfer, 45(21) (2002) 4325-4331.
[38] E.J.L. Toledo, T.C. Ramalho, Z.M. Magriotis, Influence of magnetic field on physical–chemical properties of the liquid water: Insights from experimental and theoretical models, Journal of Molecular Structure, 888(1) (2008) 409-415.
[39] J.V. Stewart, Intermediate Electromagnetic Theory, World Scientific, 2001.

HOW TO CITE THIS ARTICLE
A. Ramezani, A. Faghih Khorasani, A. Ayoobi, An investigation of pool boiling under alternating magnetic field and steady-state conditions , AUT J. Mech Eng., 7(1) (2023) 3-18.

DOI: 10.22060/ajme.2022.21605.6041